Rapid and high capacity methane storage in clathrate hydrates using surfactant dry solution

Shuanshi Fan[a], Liang Yang[a], Yanhong Wang[a,b], Xuemei Lang[a], Yonggang Wen[a,*] and Xia Lou[c]

[a] Key Lab of Enhanced Heat Transfer and Energy Conservation, Ministry of Education, School of Chemistry and Chemical Engineering, South China University of Technology, Guangzhou 510640, China

[b] The Key Laboratory of Fuel Cell Technology of Guangdong Province, Guangzhou 510640, China

[c] Department of Chemical Engineering, Curtin University, Kent Street, Bentley, WA 6102, Australia

* Corresponding author. Tel/Fax: +86 20 22236581.

E-mail address: cewenyg@scut.edu.cn (Y.G. Wen).

Abstract

Surfactant dry solution (DS) was prepared by mixing sodium dodecyl sulfate (SDS) solution, hydrophobic silica nanoparticles and air in a high speed blender. Flour-like SDS-DS combines the advantages of dispersed dry water and active SDS solution. Methane storage in clathrate hydrates using SDS-DS was investigated in a stainless steel vessel without stirring under the condition of 5.0 MPa and 273.2 K. The results demonstrated that highly dispersed SDS-DS could significantly enhance formation kinetics and storage capacity of methane hydrate. SDS-DS exhibited about the same methane storage capacity (172.96 $m^3 \cdot m^{-3}$) as dry water, but faster storage rates than dry water. Compared to SDS solution, SDS-DS had similar storage rates (7.44 $m^3 \cdot m^{-3} \cdot min^{-1}$) and higher methane storage capacity under the relative low pressure. However, the aggregation of partial SDS-DS powders destroyed its original dispersive property after hydrate dissociation.

Keywords: surfactant, dry solution, methane hydrate, formation kinetics

1. Introduction

Gas hydrates are crystalline compounds encaging noble gases or short chain hydrocarbons as guest molecules in a hydrogen-bonded water framework (Sloan and Koh, 2008). In recent years, natural gas hydrates have drawn significant attention not only as a new natural energy resource but also as a new economical medium for natural gas storage and transportation (Sloan, 2003; Englezos and Lee, 2005; Koh and Sloan, 2007). One standard volume of such hydrates can stably store about 180 standard volumes of natural gas (Sloan and Koh, 2008), which corresponds to approximately one-quarter energy density of liquefied natural gas. High storage capacity of hydrate have also contributed carbon dioxide capture (Linga et al., 2007), flue gas separation (Kang and Lee, 2000; Fan et al., 2009), hydrogen storage (Mao et al., 2002; Struzhkin et al., 2007), seawater desalination (Park et al., 2011) and solute purification (Yoon and Lee, 1997) in the form of hydrate.

However, the application on an industrial scale has been critically challenged by slow formation rate and low conversion ratio of gas to hydrate resulting in insufficient storage capacity. The causes of these problems lie in inadequate gas-water contacts and unreacted interstitial water trapped in the hydrate mass, neither of which favors hydrate nucleation and growth. Therefore, enhancing gas-water contacts is crucial for efficient hydration of gas to solid.

Mechanical methods, such as liquid stirring (Englezos et al., 1987; Hao et al., 2007), gas bubbling (Maini and Bishnoi, 1981; Luo et al., 2007), liquid spraying (Fukumoto et al., 2001; Ohmura et al., 2002), are often employed in experimental operations to increase the formation rate of gas hydrates. However, the substantial cost of mechanical mixing devices and energy

requirements may be unfeasible in real gas storage application. The addition of surfactants to water can enhance gas hydrates formation without mechanical perturbation (Zhong and Rogers, 2000; Link et al., 2003; Zhang et al., 2007). Evidently, the presence of surfactants increases gas-water contacts by changing the hydrate morphology (Yoslim et al., 2010), but the gas storage medium remains a pool of stationary liquid. Silica sand saturated with water (fixed bed column) is recently employed for enhancing the rate of gas hydrate formation and the percent of water conversion to hydrate (Linga et al., 2007). However, the volume "penalty" is high because the sand occupies quite large space in the bed column. Grinding ice powder exposed in the gas provides considerable gas-ice contacts and increases hydrate formation rates (Staykova et al., 2003), but the material must be prepared laboriously without melting. Dispersed liquid such as dry water (DW) with higher specific surface than ice powder, is used to dramatically enhance the methane uptake rate in hydrates under static conditions (Wang et al., 2008; Carter et al., 2010). Dry water can capture more methane than surfactant solution, but the enhanced rate of gas uptake is slightly inferior to the rate increased by surfactant (Carter et al., 2010).

Considering storage advantages of DW and surfactant solution, in this work, we attempt to prepare a surfactant dry solution (DS) using sodium dodecyl sulfate (SDS) solution and hydrophobic silica nanoparticles. Formation kinetic behaviors of methane hydrate in the SDS-DS were investigated under given pressure and temperature. In order to distinctly observe the effect of SDS-DS on hydration kinetics, DW and SDS solution also were used for methane hydrate formation under the same operating conditions, respectively. The results are expected to provide useful information on kinetic properties of hydrate formation in static

dispersed solution.

2. Experimental

2.1 Preparation of surfactant dry solution

Full details of the procedure for preparation of dry liquid can be referred elsewhere (Binks and Murakami, 2006). A sample of hydrophobic silica nanoparticles (HB630) with particle size range of 5~15 nm was supplied by Guangzhou GBS High-Tech & Industry Co., Ltd.. A sample of sodium dodecyl sulfate (SDS) with certified purity of >99% was purchased from Shanghai Bio Science & Technology Co., Ltd.. To prepare SDS-DS, SDS (0.03 g) was dissolved in deionized water (99.97 g) to form SDS solution beforehand. And then the solution was poured into a blender (Philips HR1727/06, 1.5 liter) and silica HB630 was added to the solution. Mixing was carried out at a speed of 18000 rpm for two 15 seconds under ambient conditions. SDS-DS sample looks like dry flour but can freely flow like liquid. Four mixing ratios of solution to silica were designed, as shown in Table 1. DW was also prepared by mixing 46.25 g of deionized water and 3.75 g of HB630 with the same operation above.

2.2 Formation of methane hydrate

Gas consumption based on pressure-volume-temperature (PVT) measurements can be considered as an efficient method to conduct laboratory experiments, which was reported in our previous paper (Yang et al., 2012). The apparatus employed in this work is shown schematically in Fig. 1. Before each experiment, a stainless steel high-pressure vessel (50 mm in diameter, 153 mm in height and effective volume of 300 cm^3, Jiangsu Hai'an Scientific Research Instrument Factory) was washed with deionized water and loaded with 15.00 g of SDS-DS (or DW or SDS solution or bulk water). Subsequently, a vacuum pump (2XZ-4,

Zhejiang Taizhou Qiujing Vacuum pump Co., Ltd.) was started to evacuate air from the apparatus, and then the vessel was flushed with methane (99.99 % purity, Guangzhou Yinglai Gases Co., Ltd) three times to ensure the absence of air. Afterwards, a circulating coolant bath (THD-3010, Zhejiang Ningbo Tianheng Instrument Factory) with a heating/cooling coil was turned on to control the vessel temperature to 273.2 K. The coolant with a freezing point lower than 243 K is prepared by blending equivalent volume of water and glycol. Two thermal resistance detectors (Pt100, ± 0.01 K, -30~200 ℃ Jiangsu Plaza Premium Electric Instrument Co., Ltd.) were used for measuring the temperatures of gas phase and liquid phase, respectively. Once the desired temperature was maintained constant for several minutes, methane was injected into the vessel until the given pressure (5.0 MPa) was reached, and then gas injection was cut off. The pressure of gas supply was monitored using a pressure gauge with a precision of ± 0.1 MPa. A pressure transducer (DG1300, ± 0.01 MPa, 0~40 MPa, Guangzhou Senex Instrument Co., Ltd.) was used for measuring the pressure in the vessel. The time, temperature and pressure information was collected (10 seconds between individual *t-T-P* points) by Agilent 34970A Data Logger (Agilent Technologies Co., Ltd.) and displayed on the computer screen. In the initial period of hydrate formation, liquid temperature increased while the gas pressure decreased obviously. When the pressure drop rate was less than 0.01 MPa over 30 min, hydration process was assumed to reach its destination. Experimental conditions of all tests conducted were listed in Table 2.

2.3 Calculation of methane storage rate and capacity

Methane storage rate and capacity during the hydration process could be determined from the *t-T-P* data. The formation rate, *F*, was defined as

$$F = \frac{\mathrm{d}\left(V_{t,\mathrm{gas}}^{\mathrm{h}}\right)_{\mathrm{STP}}}{V_t^{\mathrm{h}}\mathrm{d}t} \approx \frac{\left(\Delta V_{t,\mathrm{gas}}^{\mathrm{h}}\right)_{\mathrm{STP}}}{V_t^{\mathrm{h}}\Delta t}, \quad (1)$$

where V^{h}, $V_{\mathrm{gas}}^{\mathrm{h}}$ and $\Delta V_{\mathrm{gas}}^{\mathrm{h}}$ are the accumulative volume of hydrate phase, the volume of gas in hydrate phase and the volume increment of gas in hydrate phase in the period of Δt, respectively. The subscript *t*, as well as 0, $t+\Delta t$ and e appeared in the following equations denote the state of time *t*, the initial state, the state of time $t+\Delta t$ and the final (equilibrium) state, respectively. STP represents the standard temperature and pressure.

Zhang et al. (2005) stated that the water expends to about 1.25 times its original volume during its conversion into hydrate. Therefore, V_t^{h} is determined by the following equation:

$$V_t^{\mathrm{h}} = 1.25\alpha_t V_0^{\mathrm{l}}, \quad (2)$$

where V_0^{l} is the initial volume of liquid phase in the vessel and α is the fraction of water converted into hydrate, it is evaluated with the following equation:

$$\alpha_t = \frac{\left(V_{t,\mathrm{gas}}^{\mathrm{h}}\right)_{\mathrm{STP}}}{\left(V_{\mathrm{e,gas}}^{\mathrm{h}}\right)_{\mathrm{STP}}}, \quad (3)$$

where $\left(V_{t,\mathrm{gas}}^{\mathrm{h}}\right)_{\mathrm{STP}}$ and $\left(V_{\mathrm{e,gas}}^{\mathrm{h}}\right)_{\mathrm{STP}}$ are described by the following formulas in the unit of cm^3:

$$\left(V_{t,\mathrm{gas}}^{\mathrm{h}}\right)_{\mathrm{STP}} = 22400 n_{t,\mathrm{gas}}^{\mathrm{h}}, \ \left(V_{\mathrm{e,gas}}^{\mathrm{h}}\right)_{\mathrm{STP}} = 22400 n_{\mathrm{e,gas}}^{\mathrm{h}}, \quad (4)$$

where $n_{\mathrm{gas}}^{\mathrm{h}}$ is the molar number of gas in hydrate phase or the molar number of gas uptake during hydrate formation.

The idea unit cell formula of structure I is $2(5^{12})\cdot 6(5^{12}6^2)\cdot 46H_2O$ (Sloan and Koh, 2008). When the unit of water volume is cm^3, the mass value of water equals to its volume value. So according to the formula of structure I, $n_{\mathrm{e,gas}}^{\mathrm{h}}$ can be determined by:

$$n_{\mathrm{e,gas}}^{\mathrm{h}} = \frac{V_0^{\mathrm{l}}}{18\times 46}\left(2\theta_1 + 6\theta_2\right), \quad (5)$$

where θ_1 and θ_2 are the occupancy of gas molecules in small cavities and large cavities of

hydrate, respectively. The model of Chen and Guo is used to determine θ_1 and θ_2 (Chen and Guo, 1998).

The standard volume increment of gas in hydrate phase, $\left(\Delta V_{t,\mathrm{gas}}^{\mathrm{h}}\right)_{\mathrm{STP}}$, can be calculated by the following equations in the unit of cm^3:

$$\left(\Delta V_{t,\mathrm{gas}}^{\mathrm{h}}\right)_{\mathrm{STP}} = 22400\left(n_{t+\Delta t,\mathrm{gas}}^{\mathrm{h}} - n_{t,\mathrm{gas}}^{\mathrm{h}}\right), \tag{6}$$

$$n_{t,\mathrm{gas}}^{\mathrm{h}} = n_0^{\mathrm{g}} - n_t^{\mathrm{g}}, \quad n_{t+\Delta t,\mathrm{gas}}^{\mathrm{h}} = n_0^{\mathrm{g}} - n_{t+\Delta t}^{\mathrm{g}}, \tag{7}$$

where $n_{\mathrm{gas}}^{\mathrm{h}}$ and n^{g} represents the molar number of gas in hydrate phase and the molar number of gas phase, respectively. n_0^{g}, n_t^{g} and $n_{t+\Delta t}^{\mathrm{g}}$ can be determined by:

$$n_0^{\mathrm{g}} = \frac{P_0 V_0^{\mathrm{g}}}{Z_0 R T_0}, \quad n_t^{\mathrm{g}} = \frac{P_t V_t^{\mathrm{g}}}{Z_t R T_t}, \quad n_{t+\Delta t}^{\mathrm{g}} = \frac{P_{t+\Delta t} V_{t+\Delta t}^{\mathrm{g}}}{Z_{t+\Delta t} R T_{t+\Delta t}}, \tag{8}$$

where P, T, V^{g} and Z are the pressure, the temperature, the volume of gas phase and the gas compressibility factor, respectively. The compressibility factor Z is calculated with Redlich-Kwong equation (Redlich and Kwong, 1949). V_0^{g} can be described by:

$$V_0^{\mathrm{g}} = V_{\mathrm{vessel}} - V_0^{\mathrm{l}} - V^{\mathrm{Si}}, \tag{9}$$

where V_{vessel} is the volume of the pressure vessel and V^{Si} is the volume of solid silica particles. V^{Si} can be calculated indirectly by the mass of silica HB630 and its density of 2.2 $\mathrm{g \cdot cm^{-3}}$. In view of the volume expansion of solution and the constant volume of pressure vessel, the increasing volume of the condensed phase (liquid and hydrate) will occupy the gas phase space. It leads to the decrease of the gas phase volume correspondingly. So the volume of gas phase, V_0^{g}, should be corrected by:

$$V_t^{\mathrm{g}} = V_0^{\mathrm{g}} - 0.25\alpha_t V_0^{\mathrm{l}}, \quad V_{t+\Delta t}^{\mathrm{g}} = V_0^{\mathrm{g}} - 0.25\alpha_{t+\Delta t} V_0^{\mathrm{l}}, \tag{10}$$

where α is calculated by Eq. (3) and Eq. (4).

The storage capaticy, C, can be obtained conveniently with the equation of $C = \frac{\left(V_{t,\mathrm{gas}}^{\mathrm{h}}\right)_{\mathrm{STP}}}{V_t^{\mathrm{h}}}$ together with above equations.

3. Results and discussion

3.1 Surfactant dry solution preparation and morphology

SDD-DS is solution droplets-in-air inverse foam formed by mixing SDS solution, hydrophobic silica nanoparticles and air in a high speed blender. Fig. 2 illustrates schematically the transition from bulk solution to micro-droplets in the presence of silica particles. Hydrophobic silica particles can encapsulate isolated macroscopic SDS solution droplets in air. Highly dispersed SDS-DS droplets are like solid flour powder (upper right in Fig. 2), but its water content is more than 90 wt%. The bulk density of SDS-DS was measured to be about 0.55~0.60 g·cm^{-3}. Not only SDS-DS droplets can provide plenty of gas-liquid contacts, but also each droplet encapsulated by HB630 can be considered as a micro hydration system containing surfactant. Therefore, SDS-DS is expected to have better enhanced effects on hydrate formation than single DW or single SDS solution. Additionally, the SDS-DS has high stability and its good dispersive property can be maintained for around 6 months at room temperature.

The morphology of SDS-DS droplets with altered silica contents can be distinguished in an inverted optical microscope (Carl Zeiss Axio Observer A1) with an accuracy of 1 μm. Photographs were taken with a digital camera (IMAGING Micro-Publisher 5.0RTV). The particle size of SDS-DS droplets was measured using an attendant graphics-software of the optical microscope. The sample with 7.5 wt% silica particles (Fig. 3c) had uniform particle size, narrow size range (1~2 μm) and ample specific surface. Solution droplets with similar

particle size existed in the sample with 10.0 wt% silica particles (Fig. 3d), but excess fumed silica particles were intermixed with droplets. By comparison, the particle size of sample with 5.0 wt% fumed silica particles (Fig. 3b) was nonuniform and ranged from 3μm to 10 μm. The sample with 2.5 wt% fumed silica particles (Fig. 3a) exhibited very poor dispersion, such as irregular shape and large droplet size with the range of 15~120 μm. Excess solution resulted in large droplets due to coalescence. The particle size of SDS-DS droplets with above four silica contents is shown in Fig. 4.

3.2 Methane hydrate formation

For all the SDS-DS systems in the work, every pressure curves and temperature curves exhibit similar changes. Take SDS-DS system (7.5 wt% silica HB630) for an example, typical variations of gas pressure and liquid temperature with time for hydration systems of bulk water and SDS-DS are shown in Fig. 5. The vessel was pressurized to 5.0 MPa at the temperature of 273.2 K. In the bulk water system, there was no clear evidence (pressure drop and temperature rise) that methane hydrate was formed under the conditions. By contrast, when the dispersed SDS-DS was employed, dramatic methane pressure drop together with SDS-DS temperature rise occurred at an induction time of 8.2 min. It was an indication of the start of methane hydrate formation and a solid hydrate layer was formed at gas-droplet interface. As the hydrate grew, the pressure gradually decreased, meanwhile the temperature increased rapidly to a maximum and then decreased to the initial temperature. When the hydrate layer developed to a thick wall on the surface of SDS-DS droplets, there was no hydrate formation and methane pressure stopped decrease. The rapid gas consumed in SDS-DS can compete with (even surpass) that reported for methane enclathration in dry water

under 8.6 MPa (Wang et al., 2008) which is higher than our test pressure. The behavior may be attributed to the highly dispersed SDS solution which provides sufficient gas-liquid contact area during hydrate nucleation and growth.

3.3 Methane storage rate and capacity

Kinetics of methane uptake in SDS-DS samples with altered contents of silica HB630 under 5.0 MPa and 273.2 K is described in Fig. 6. Methane uptake in the bulk water only approached to about 7.0 $m^3 \cdot m^{-3}$ during the whole experimental process. Few contacts of water molecules and methane molecules should be the main cause of little hydration. However, there are drastic increase gas consumptions in all the SDS-DS systems (2.5 wt%~10.0 wt% HB630). At the beginning of 40 min, the curves of methane uptakes nearly close to straight lines with about the same slope for these SDS-DS systems. Gas storage capacities reach their maximum values (more than 150 $m^3 \cdot m^{-3}$) within about 100 min. Methane uptake rates, slopes of capacity curves, are shown in the inner plots of Fig. 6. Methane hydration rate in the bulk water system nearly approached to 0, while in SDS-DS systems all hydration rates increase their maximum (more than 7.0 $m^3 \cdot m^{-3} \cdot min^{-1}$) and then tend to 0. The maximum capacity and rate for each system are listed in Table 2. The silica HB630 contents (or droplets size) of SDS-DS has no obvious effects on the kinetics of methane uptake, but the methane storage capacity of the sample with 7.5 wt% silica particles was superior to that of other DS samples. The SDS-DS sample with the highest capacity exhibits better dispersion (smaller particle size, less free fumed silica particles and less free liquid water) than other samples, which is stated in Fig. 3. The large specific surface and active droplets of SDS-DS significantly contribute to the enhancement of rate and capacity.

Fig. 7 shows the comparison of methane uptake kinetics in SDS solution, DW and SDS-DS (7.5 wt% silica) under the initial pressure of 5.0 MPa (T = 273.2 K). The bulk solution had the same concentration of SDS as the solution used for preparing SDS-DS. The DW kept identical with the silica content of the SDS-DS. These three systems all greatly increased the formation rate and storage capacity of hydrate compared to the bulk water system in Fig. 6. The use of SDS solution can increase gas-water contacts by changing hydrate morphology and enhance methane uptake kinetics (Yoslim et al., 2010). The dispersed DW also provided sufficient gas-water contacts for methane hydrate formation. However, the SDS-DS showed more outstanding storage performance compared to DW and SDS solution (Table 2). SDS-DS exhibited about the same methane storage capacity as DW, but faster storage rates (the inner plots in Fig. 7) than DW. The time to achieve 90% of this perfect capacity (t_{90}) under 5.0 MPa for SDS-DS was about 60 min, which was less than that of DW (200 min) with the same silica content, and also less than that reported for methane storage in DW (160 min) under 8.6 MPa (Wang et al., 2008). SDS-DS has similar storage rates as SDS solution, while it can capture more volumes of methane than SDS solution. Therefore, highly dispersed SDS-DS system combines storage advantages of dispersed DW and active SDS solution, and has dual enhancement effects on methane hydrate formation. Enhancements of storage capacity and formation rate should probably be attributed to better dispersion and surface active of SDS-DS sample. However, the aggregation of partial SDS-DS powders destroyed its original dispersive property after hydrate dissociation. As can be seen in Fig. 8, after one time hydration and dissociation, some SDS-DS droplets (7.5 wt% silica) aggregated and formed partial continuous bulk water.

In order to illustrate SDS-DS's enhancing hydration and micro-droplet aggregation, a hypothesis of methane hydrate formation and dissociation in SDS-DS system was raised in Fig. 9. In the SDS-DS system, micro-droplets with a size of 1~2 μm were encapsulated by hydrophobic silica nanoparticles and kept isolated each other (Fig. 9A). Dispersed SDS-DS contributed abundant gas transport and gas-water interfacial surface area to hydrates nucleation and growth. For each solution droplet, it can be taken as a miniature hydration system based on SDS solution. During hydration process, thin methane hydrate layer formed around the surface of droplets (Fig. 9B) and grew thick gradually (Fig. 9C). Previous studies have reported that branches of porous fibre-like hydrate were formed in the presence of surfactants and increased gas-water contacts for further hydrate crystals growth (Yoslim et al., 2010). Thus SDS-DS system has dispersion of DW and surface active of SDS. Especially, SDS-DS sample (7.5 wt% silica) with better dispersion enhanced more gas-water contacts than other samples and stored the most methane. Solution droplets expanded during their conversion into hydrate, so adjacent hydrate particles would freeze each other until the end of hydration (Fig. 9D). When hydrate dissociation, freezing hydrate particles melted and aggregated to bigger droplets. Partial aggregated bigger droplets became continuous solution (Fig. 8) and could not recover their original isolated droplets again. Stabilized surfactant-DS with enhancement effect on hydration will be further investigated.

4. Conclusion

In summary, we use the highly dispersed surfactant-DS as a storage medium to significantly improve methane uptake kinetics and storage capacity for the first time. Surfactant-DS combines the advantages of dispersed DW and active SDS solution. Not only

our SDS-DS can provide considerable gas-liquid contacts, but also each droplet is a micro hydration system with surfactant. SDS-DS system can store methane faster compared to DW and has higher storage capacity compared to SDS solution under a relative low pressure. The results will provide useful information on kinetics of gas to solid hydrate in static dispersed solution. However, after freezing hydration and warming dissociation, SDS-DS droplets aggregate to bigger droplets and even form partial continuous solution. The destroyed droplets cannot recover their original dispersive state, so further study will be focused on stabilized surfactant-DS.

Acknowledgments

We thank the financial support from the National Natural Science Foundation of China (Grant No. 51176051 and 51106054), the Fundamental Research Funds for the Central University (No. 2013ZM0036 and No. 2013ZZ0032), PetroChina Innovation Foundation (No. 2012D-5006-0210 and 2013D-5006-0107), and research fund of the Key Laboratory of Fuel Cell Technology of Guangdong Province.

Notation

C gas capacity, $m^3 \cdot m^{-3}$

F hydrate formation rate, $m^3 \cdot m^{-3} \cdot min^{-1}$

n molar number of gas, mol

P pressure, MPa

R universal gas constant, 8.3145 J/mol/K

t time, min

T absolute temperature, K

V volume, cm^3

Z gas compressibility factor

Greek letters

α fraction of water converted into hydrate, %

θ occupancy of gas molecules in hydrate cavities

Δt time interval of two states, min

ΔV volume increment, cm^3

Subscripts

0 initial state

1 small cavities of hydrate

2 large cavities of hydrate

90 gas consumption reaches 90 % of final storage capacity

e final (equilibrium) state

t state of time t

STPstandard temperature and pressure

Superscripts

g gas phase

h hydrate phase

l liquid phase

Si hydrophobic silica HB630

References

Binks, B.P., Murakami, R., 2006. Phase inversion of particle-stabilized materials from foams to dry water. Nat. Mater. 5, 865–869.

Carter, B.O., Wang, W.X., Adams, D.J., Cooper, A.I., 2010. Gas storage in “dry water” and “dry gel” clathrates. Langmuir 26, 3186–3193.

Chen, G.J., Guo, T.M., 1998. A new approach for gas hydrate modeling. Chem. Eng. J. 71, 145–151.

Englezos, P., Kalogerakis, N., Dholabhai, P.D., Bishnoi, P.R., 1987. Kinetics of formation of methane and ethane gas hydrates. Chem. Eng. Sci. 42, 2647–2658.

Englezos, P., Lee, J.D., 2005. Gas hydrates: a cleaner source of energy and opportunity for innovative technologies. Korean J. Chem. Eng. 22, 671–681.

Fan, S.S., Li, S.F., Wang, J.Q., Lang, X.M., Wang, Y.H., 2009. Efficient Capture of CO_2 from Simulated Flue Gas by Formation of TBAB or TBAF Semiclathrate Hydrates. Energy Fuels 23, 4202–4208.

Fukumoto, K., Tobe, J., Ohmura, R., Mori, Y.H., 2001. Hydrate formation using water spraying in a hydrophobic gas: a preliminary study. AIChE J. 47, 1899–1904.

Hao, W.F., Wang, J.Q., Fan, S.S., Hao, W.B., 2007. Study on methane hydration process in a semi-continuous stirred tank reactor. Energy Convers. Manage. 48, 954–960.

Kang, S.P., Lee, H., 2000. Recovery of CO_2 from flue gas using gas hydrate: thermodynamic verification through phase equilibrium measurements. Environ. Sci. Technol. 34, 4397–4400.

Koh, C.A., Sloan, E.D., 2007. Natural gas hydrates: recent advances and challenges in energy

and environmental applications. AIChE J. 53, 1636–1643.

Linga, P., Kumar, R., Englezos, P., 2007. The clathrate hydrate process for post and pre-combustion capture of carbon dioxide. J. Hazard. Mater. 149, 625–629.

Link, D.D., Ladner, E.P., Elsen, H.A., Taylor, C.E., 2003. Formation and dissociation studies for optimizing the uptake of methane by methane hydrates. Fluid Phase Equilibr. 211, 1–10.

Luo, Y.T., Zhu, J.H., Fan, S.S., Chen, G.J., 2007. Study on the kinetics of hydrate formation in a bubble column. Chem. Eng. Sci. 62, 1000–1009.

Maini, B.B., Bishnoi, P.R., 1981. Experimental investigation of hydrate formation behavior of a natural gas bubble in a simulated deep sea environment. Chem. Eng. Sci. 36, 183–189.

Mao, W.L., Mao, H.K., Goncharov, A.F., Struzhkin, V.V., Guo, Q., Hu, J., Shu, J., Hemley, R.J., Somayazulu, M., Zhao, Y., 2002. Hydrogen clusters in clathrate hydrate. Science 297, 2247–2249.

Ohmura, R., Kashiwazaki, S., Shiota, S., Tsuji, H., Mori, Y.H., 2002. Structure-I and structure-H hydrate formation using water spraying. Energy Fuels 16, 1141–1147.

Park, K., Hong, S.Y., Lee, J.W., Kang, K.C., Lee, Y.C., Ha, M.G., Lee, J.D., 2011. A new apparatus for seawater desalination by gas hydrate process and removal characteristics of dissolved minerals (Na^+, Mg^{2+}, Ca^{2+}, K^+, B^{3+}). Desalination 274, 91–96.

Redlich, O., Kwong, J.N.S., 1949. On the thermodynamics of soloutions. V an equation of state, Fugacities of gaseous solutions. Chem. Rev. 44, 233–244.

Sloan, E.D., 2003. Fundamental principles and applications of natural gas hydrates. Nature 426, 353–359.

Sloan, E.D., Koh, C.A., 2008. Clathrate Hydrates of Natural Gases, third ed. CRC Press–Taylor & Francis, Boca Raton, FL.

Staykova, D.K., Kuhs, W.F., Salamatin, A.N., Hansen, T., 2003. Formation of porous gas hydrates from ice powders: diffraction experiments and multistage model. . Phys. Chem. B 107, 10299–10311.

Struzhkin, V.V., Militzer, B., Mao, W.L., Mao, H.K. Hemley, R.J., 2007. Hydrogen storage in molecular clathrates. Chem. Rev. 107, 4133−4151.

Wang, W.X., Bray, C.L., Adams, D.J., Cooper, A.I., 2008. Methane storage in dry water gas hydrates. Journal of the American Chemical Society 130, 11608–11609.

Yang, L., Fan, S.S., Wang, Y.H., Lang, X.M., Xie, D.L., 2011. Accelerated formation of methane hydrate in aluminum foam. Ind. Eng. Chem. Res. 50, 11563– 11569.

Yoon, J.H., Lee, H., 1997. Clathrate phase equilibria for the water-phenol-carbon dioxide system. AIChE J. 43, 1884–1893.

Yoslim, J., Linga, P., Englezos, P., 2010. Enhanced growth of methane–propane clathrate hydrate crystals with sodium dodecyl sulfate, sodium tetradecyl sulfate, and sodium hexadecyl sulfate surfactants. J. Cryst. Growth 313, 68–80.

Zhang, J.S., Lee, S., Lee, J.W., 2007. Kinetics of methane hydrate formation from SDS solution. Ind. Eng. Chem. Res. 46, 6353–6359.

Zhang, L.W., Chen, G.J., Sun, C.Y., Fan, S.S., Ding, Y.M., Wang, X.L., Yang, L.Y., 2005. The partition coefficients of ethylene between hydrate and vapor for methane + ethylene + water and methane + ethylene + SDS + water systems. Chem. Eng. Sci. 60, 5356–5362.

Zhong, Y., Rogers, R.E., 2000. Surfactant effects on gas hydrate formation. Chem. Eng. Sci.

55, 4175–4187.

Captions

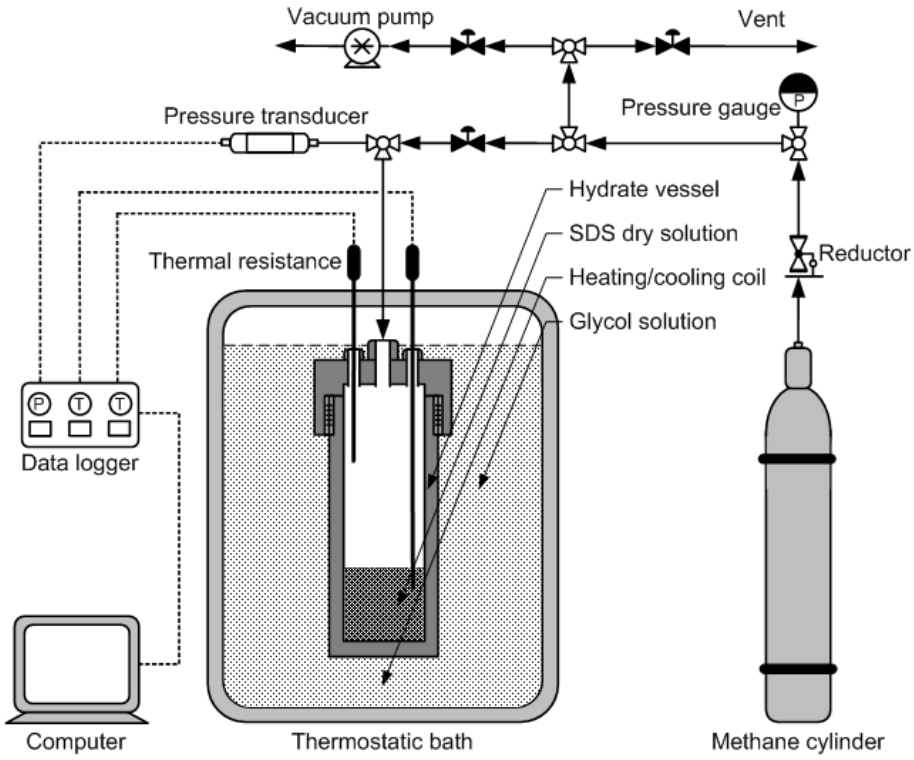

Fig. 1. Schematic diagram of experimental apparatus.

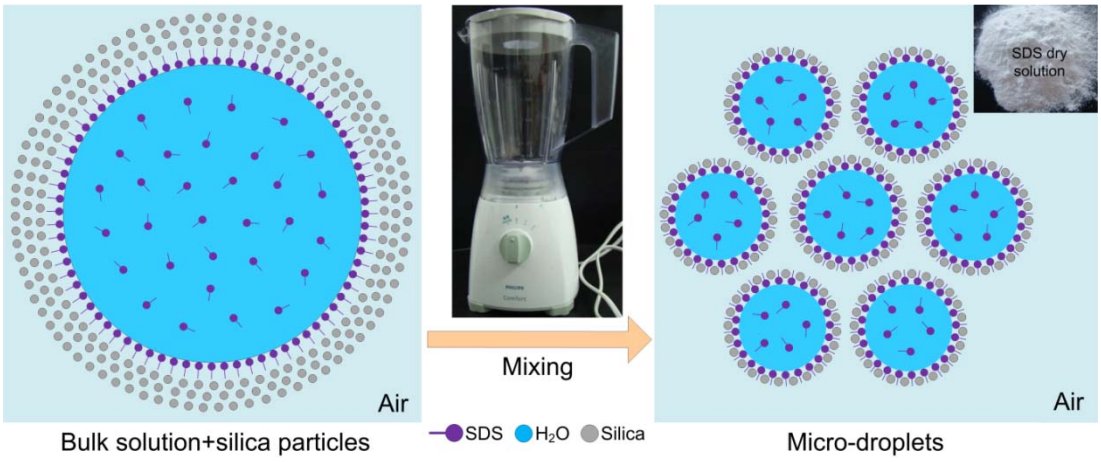

Fig. 2. Schematic illustration of the preparation of SDS solution droplets. Free-flowing SDS-DS powder (upper right) formed by aerating 46.25 g of 0.03 wt% SDS solution and 3.75 g of hydrophobic silica nanoparticles HB630 at 18000 rpm for two 15 seconds.

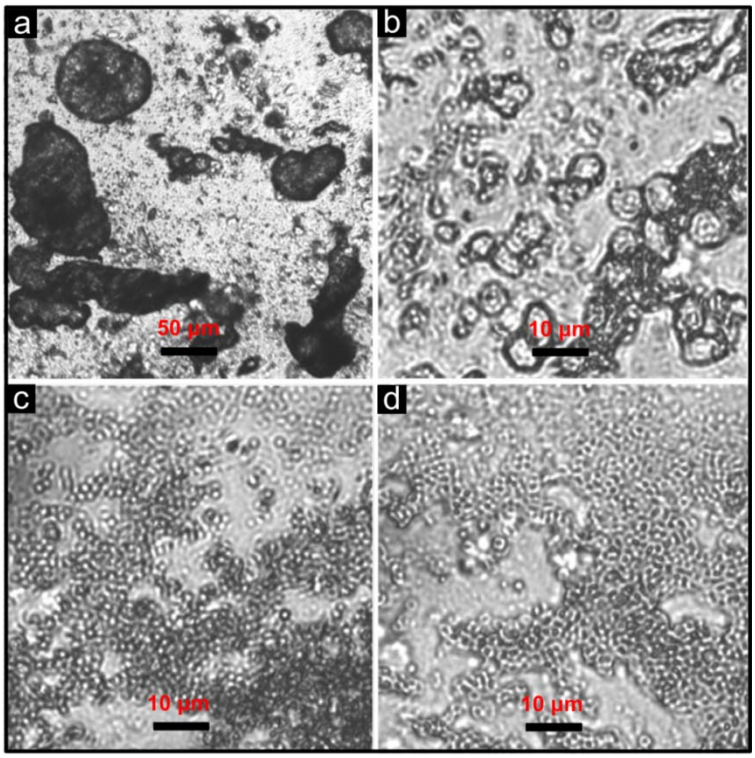

Fig. 3. Optical micrographs of SDS-DS droplets with (a) 2.5 wt%, (b) 5.0 wt%, (c) 7.5 wt%, (d) 10.0 wt% hydrophobic silica particles HB630.

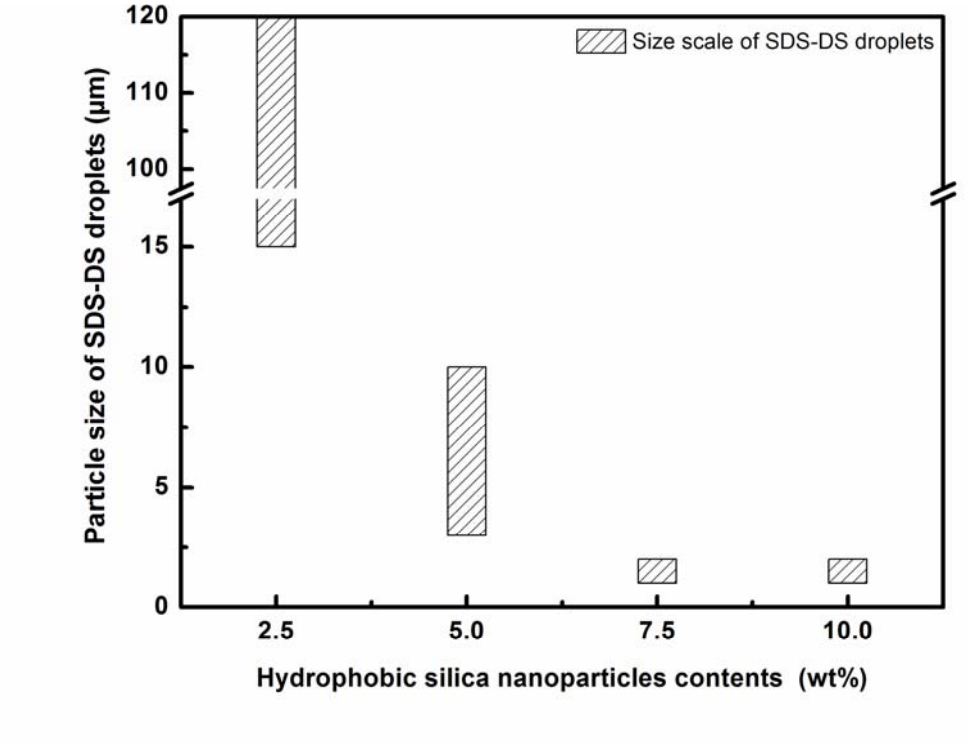

Fig. 4. Particle size of SDS-DS droplets with altered contents of silica particles.

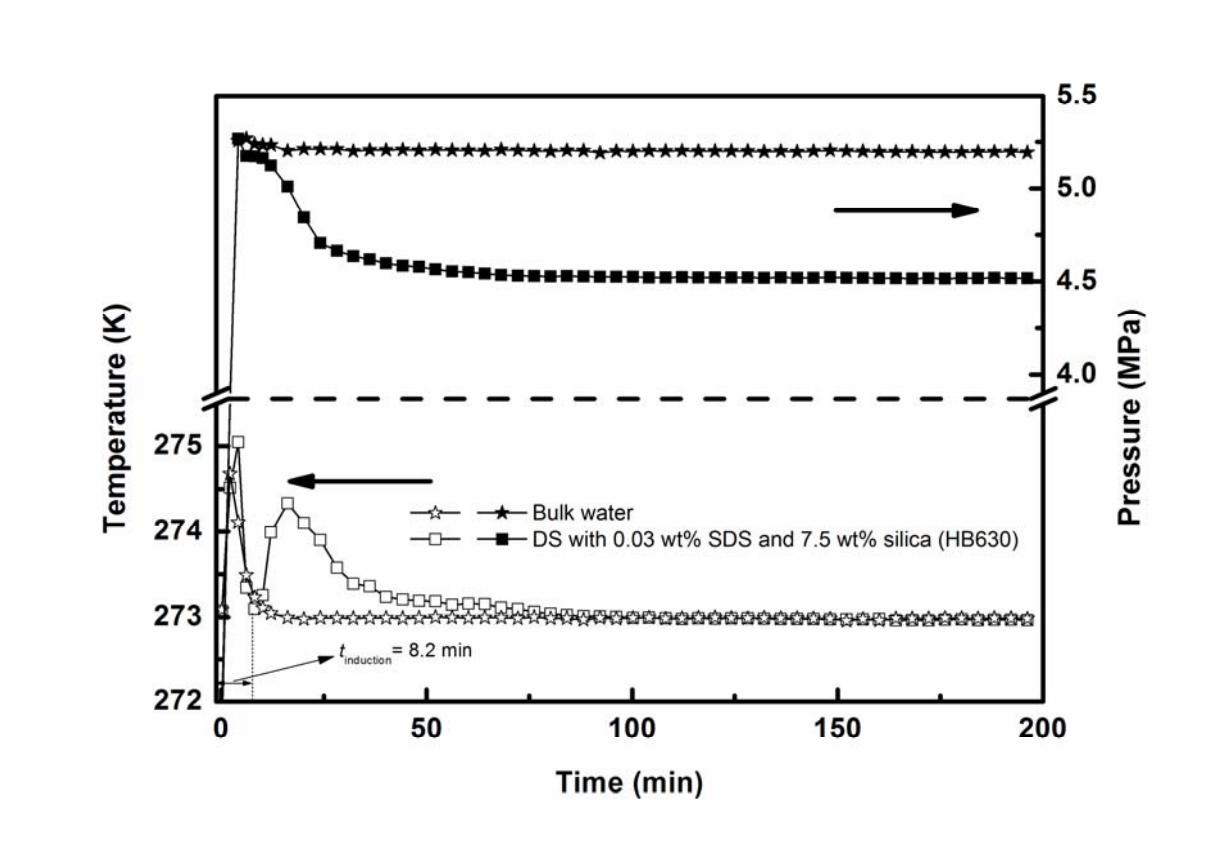

Fig. 5. Variations of methane pressure and liquid temperature with time during hydrate formation in bulk water and SDS-DS.

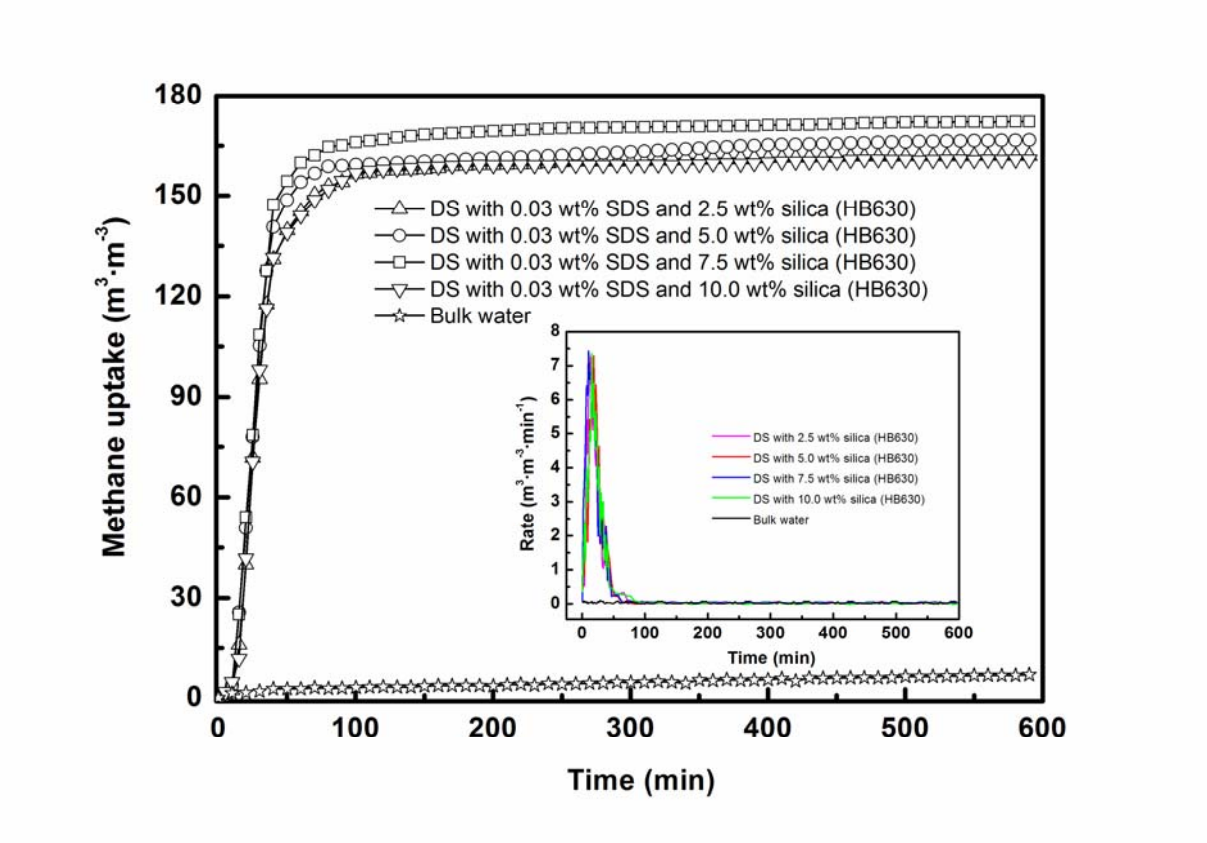

Fig. 6. Kinetics of methane uptake in SDS-DS systems with altered contents of silica particles (HB630) under the initial pressure of 5.0 MPa (T = 273.2 K).

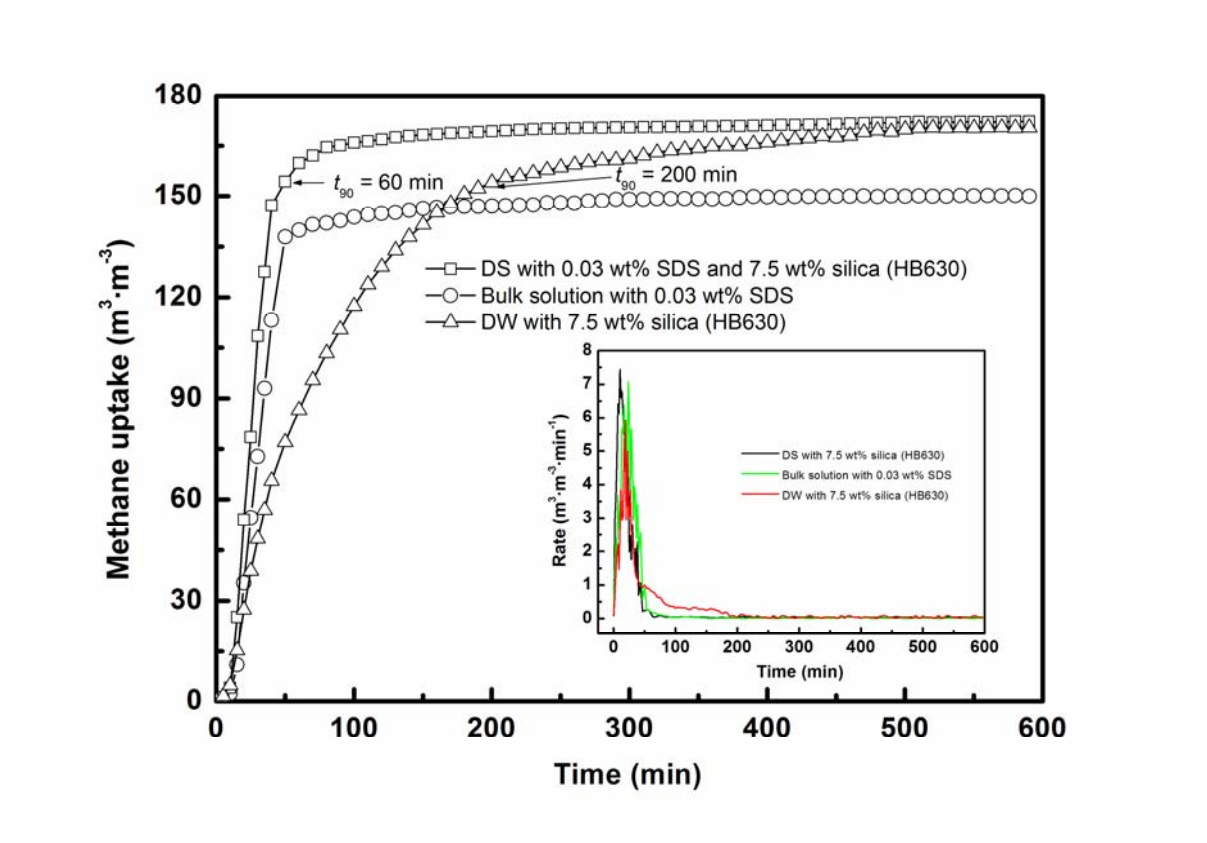

Fig. 7. Kinetics of methane uptake in bulk SDS solution, DW and SDS-DS under the initial pressure of 5.0 MPa (T = 273.2 K).

Fig. 8. Aggregation of SDS-DS (7.5 wt% silica) after one time hydration and dissociation.

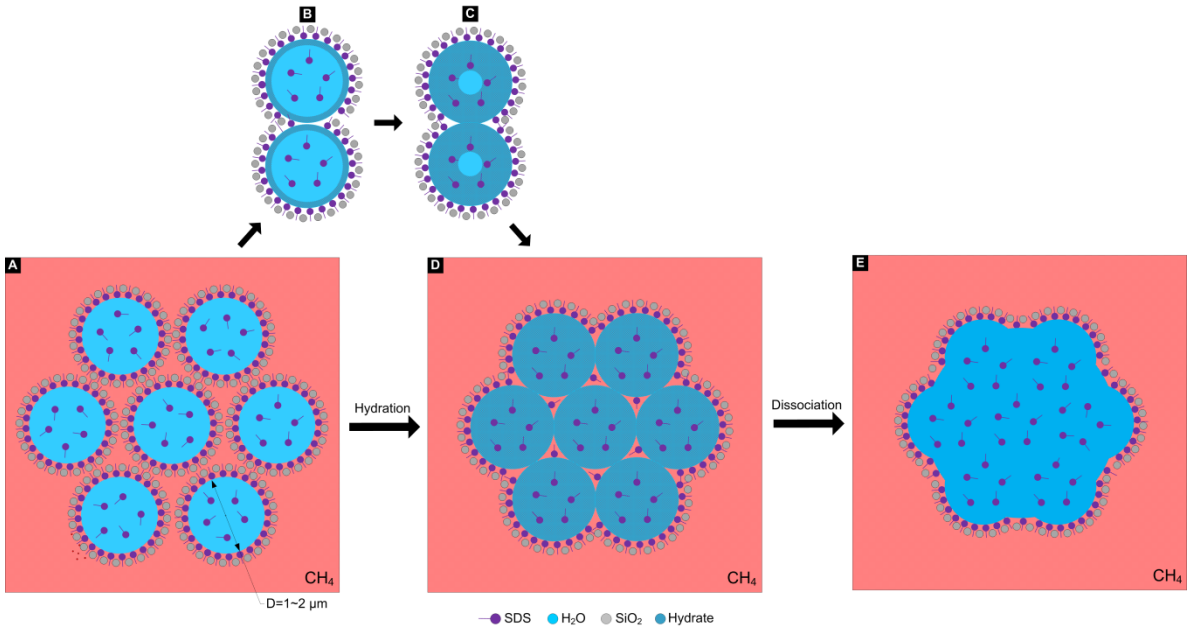

Fig. 9. Schematic illustration of methane hydrate formation and dissociation in SDS-DS system. (A) SDS-DS droplets exposed in methane phase, (B~C) growth of methane hydrate layer formed around droplets surface, (D) freezing hydrate particles, (E) aggregation of droplets after hydrate dissociation.

Table 1. Mixing ratios of 0.03 wt% SDS solution to silica HB630 for preparing SDS-DS.

SDS solution weight (g)	Silica weight (g)	Silica contents (wt %)
48.75	1.25	2.5
47.50	2.50	5.0
46.25	3.75	7.5
45.00	5.00	10.0

Table 2. Experimental conditions and methane storage properties of all the systems.

Samples[1]	Weight (g)	Pressure (MPa)	Temperature (K)	Capacity[2] ($m^3 \cdot m^{-3}$)	Maximum rate ($m^3 \cdot m^{-3} \cdot min^{-1}$)
Bulk water	15.00	5.0	273.2	~7.00	~0
SDS solution	15.00	5.0	273.2	150.02	7.07
DW (7.5 wt% SiO_2)	15.00	5.0	273.2	170.56	5.90
SDS-DS (2.5 wt% SiO_2)	15.00	5.0	273.2	161.89	7.26
SDS-DS (5.0 wt% SiO_2)	15.00	5.0	273.2	167.32	7.29
SDS-DS (7.5 wt% SiO_2)	15.00	5.0	273.2	172.96	7.44
SDS-DS (10.0 wt% SiO_2)	15.00	5.0	273.2	160.80	7.36

[1] Concentrations of SDS in its solution and its dry solution systems are 0.03 wt%.

[2] Each group of *t*-*T*-*P* points determines an instantaneous capacity value. Each capacity listed above is the average value of the last 15 instantaneous capacity values for each test (experimental time: 600 min; data-collection interval: 10 s). The error between each average value and each one of the last 15 capacity values is ±0.15 $m^3 \cdot m^{-3}$, which is acceptable in our

tests.